

Competing Ordering Modes in the Distorted Quantum Kagome Material Clinoatacamite $\text{Cu}_2\text{Cl}(\text{OH})_3$

L. Stödter,^{1, 2, *} C. Kastner,¹ H. O. Jeschke,³ M. Reehuis,⁴ K. Beauvois,⁵ B. Ouladdiaf,⁵ E. Chan,⁵ F. Yokouchi,^{4, †} F. Bert,⁶ T. J. Hicken,⁷ J. A. Krieger,⁷ H. Luetkens,⁷ J. L. Allen,⁸ R. Feyerherm,⁴ M. Tovar,⁴ D. Menzel,¹ A. U. B. Wolter,⁹ B. Büchner,^{9, 10} K. C. Rule,¹¹ F. J. Litterst,¹ U. K. Rößler,⁹ and S. Süllow¹

¹ Institut für Physik der Kondensierten Materie, Technische Universität Braunschweig, 38106 Braunschweig, Germany

² Jülich Center for Neutron Science (JCNS) at Heinz Maier-Leibnitz Zentrum (MLZ),

Forschungszentrum Jülich GmbH, 85748 Garching, Germany

³ Research Institute for Interdisciplinary Science, Okayama University, Okayama 700-8530, Japan

⁴ Helmholtz-Zentrum Berlin für Materialien und Energie GmbH, 14109 Berlin, Germany

⁵ Institut Laue-Langevin, 38042 Grenoble Cedex 9, France

⁶ Université Paris-Saclay, CNRS, Laboratoire de Physique des Solides, 91405 Orsay, France

⁷ PSI Center for Neutron and Muon Sciences, 5232 Villigen PSI, Switzerland

⁸ Institute for Superconducting and Electronic Materials and School of Physics, University of Wollongong, NSW 2522, Australia

⁹ Leibniz Institute for Solid State and Materials Research IFW Dresden, 01069 Dresden, Germany

¹⁰ Institut für Festkörper- und Materialphysik and Würzburg-Dresden Cluster of Excellence ct.qmat, Technische Universität Dresden, 01062 Dresden, Germany

¹¹ Australian Nuclear Science and Technology Organisation, Lucas Heights, NSW 2234, Australia

(Dated: January 30, 2026)

We have studied the magnetic properties of clinoatacamite $\text{Cu}_2\text{Cl}(\text{OH})_3$, the parent compound of the quantum spin liquid candidate herbertsmithite and a longstanding puzzle among frustrated quantum magnets. As we reveal using density-functional theory, clinoatacamite belongs to the class of distorted kagome antiferromagnets with the kagome plane being embedded into a low-symmetry crystal structure. By means of thermodynamic measurements, muon spin rotation/relaxation as well as neutron diffraction on single crystals, we find a complex sequence of phases/regions below 18.1 K in zero magnetic field. We propose this complexity in multicritical clinoatacamite to arise from the competition of antiferromagnetic ordering modes from the underconstrained manifold of modes, which can lead to a metamagnetic texture in zero magnetic field.

For decades, experimental research on antiferromagnetic (AFM) quantum kagome materials has been primarily driven by the hunt for the quantum spin liquid (QSL) ground state [1, 2]. Yet, despite immense efforts, this highly entangled quantum spin state turned out to be hard to observe in real materials. Notably, the mineral herbertsmithite $\text{ZnCu}_3(\text{OH})_6\text{Cl}_2$ stands out from this research on kagome magnetic insulators as a promising QSL candidate with the absence of magnetic order or spin freezing down to mK temperatures [3–5]. This experimental observation motivated the research on an entire family of kagome materials as well as the synthesis of several new kagome compounds [6–14]. In effect, the years have shown that the sought-after QSL state is extremely unstable: Most $S = 1/2$ kagome materials adopt static order instead of QSL behavior, and, to date, it has remained unclear what defines in detail the boundary between static order and highly correlated disorder.

More recently, another direction of kagome research has formed, which explicitly turns towards *distorted* quantum kagome materials featuring a non-uniform motif of exchange couplings. It has been demonstrated that such a non-uniformity of the kagome lattice can lead to non-QSL but still exotic (quantum) behavior as, for instance, patterned valence-bond solid states [15, 16], coplanar order [13, 17], trimer networks [18] and unusual applied-field properties such as magnetization

plateaus [19]. Some of these properties have no counterpart in the uniform, ideal AFM kagome lattice described by the Hamiltonian

$$\mathcal{H} = J \sum_{\langle i,j \rangle} \mathbf{S}_i \cdot \mathbf{S}_j. \quad (1)$$

Here, J denotes the exchange interaction between nearest-neighbor (NN) spins on the corner-sharing spin triangles and $\mathbf{S}_{i,j}$ are the spin operators at sites i, j .

Distortions of a spin lattice impair the equivalence of magnetic sites. At first sight, this should lift the underconstrained nature of a kagome antiferromagnet and select distinct ordering modes. However, the manifold of ordering modes may decompose into a system of modes pertaining to different symmetries. Their competition can reestablish magnetic frustration at a higher level, resulting in complex magnetic behavior. In the present study, we address the unusual magnetic properties of one such system, clinoatacamite $\text{Cu}_2\text{Cl}(\text{OH})_3$, a distorted kagome material and a longstanding puzzle [20] in frustrated quantum magnetism. As parent compound of the paratacamite family $\text{Zn}_x\text{Cu}_{4-x}\text{Cl}_2(\text{OH})_6$, clinoatacamite ($x = 0$) is closely related to herbertsmithite ($x = 1$), but its kagome motif of Cu sites is embedded into a low-symmetry crystal structure with different site symmetries for the kagome sites. Further, unlike the QSL candi-

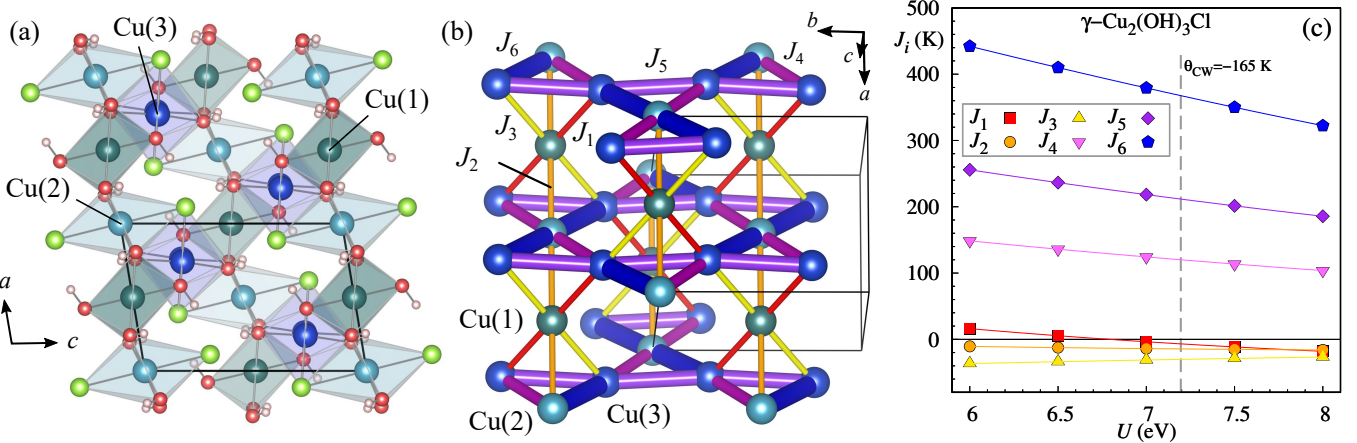


FIG. 1. (a) Crystal structure of clinoatacamite [33] viewed along the b axis [Cu(1): teal, Cu(2): light blue, Cu(3): dark blue, Cl: green, O: red, H: white]. (b) Motif of NN Cu-Cu exchange interactions J_1 – J_6 and (c) their strength derived by means of DFT and GGA+ U , plotted as function of the on-site Coulomb repulsion U . At $U = 7.19$ eV, the mean-field Curie-Weiss temperature agrees with the experimental value $\Theta_{\text{CW}} = -165(1)$ K with $J_1 = -6.8$ K, $J_2 = -14.5$ K, $J_3 = -30.3$ K, $J_4 = 120.1$ K, $J_5 = 211.6$ K and $J_6 = 367.7$ K (details in Ref. [34]). In panels (a) and (b), the unit cells are indicated.

date herbertsmithite, clinoatacamite undergoes a magnetic transition at 18.1 K [20].

Although actively discussed in the context of kagome physics in the past [21–27], the ground states of clinoatacamite have remained inconclusive [28], in part because of the lack of single-crystal studies. In this Letter, employing density-functional theory (DFT) we will first demonstrate that clinoatacamite can be understood as a non-uniform kagome antiferromagnet with weak ferromagnetic (FM) couplings to the interlayer Cu sites. Hence, it clearly distinguishes itself from other kagome materials in the atacamite family [8] leading to a weak network of kagome planes and interlayer sites. We will further demonstrate using thermodynamic as well as microscopic measurement techniques and single-crystalline samples that clinoatacamite undergoes a complex zero-field sequence of magnetic states below 18.1 K, with further anomalies of thermodynamic quantities at 6.4 K, 6.2 K and 4.6 K: The oscillating zero-field muon spin rotation/relaxation (μSR) asymmetry reveals long-range order in all temperature regions below the 18.1 K transition. Here, the region for $T < 6.4$ K is characterized by an AFM $\mathbf{q}_m = (0, 0, 0)$ state with weak spin canting, and we find simultaneous odd-even AFM ordering modes implying a metamagnetic texture [31] in zero field.

Clinoatacamite crystallizes in a monoclinic structure of space group $P2_1/n$ (No. 14) [32] and with lattice parameters $a = 6.1675(7)$ Å, $b = 6.8327(8)$ Å, $c = 9.1517(4)$ Å and $\beta = 99.492(2)^\circ$ [33] [Fig. 1(a)]. Three inequivalent copper sites Cu(1)–Cu(3) are present. As depicted in Fig. 1(a), Cu(1)(OH)₆ and Cu(2)(OH)₄Cl₂ octahedra alternate along the a axis. Cu(3)(OH)₄Cl₂ octahedra form chains along the b axis. The Cu(2) and Cu(3) sites form a slightly distorted kagome motif, spanned by the [010] and [101] crystal directions. Cu(1) sites are in-

terlayer sites. There are three inequivalent NN Cu-Cu exchange paths (J_4 – J_6) within the kagome layers and three inequivalent NN Cu-Cu exchange paths (J_1 – J_3) between kagome and interlayer sites [Fig. 1(b)].

We show that the kagome motif is formed by the dominant exchange couplings by employing DFT with full potential local orbital basis [39] and generalized gradient approximation (GGA) functional [40]. Electronic correlations on the Cu²⁺ ions were accounted for by GGA+ U [41]. As the strength of the exchange couplings is well known to sensitively depend on Cu–O–Cu bond angles, we have first studied the crystal structure of clinoatacamite using single-crystal neutron diffraction. We collected the data using the Four-Circle Diffractometer E5 at the BER II reactor of the Helmholtz-Zentrum Berlin für Materialien und Energie (HZB), Germany [34, 42–45]. Subsequently, we used the obtained positional parameters as input for the DFT-based analysis together with lattice parameters from Ref. [33]. Fig. 1(c) visualizes the U dependence of J_1 – J_6 . Next-nearest neighbor exchanges J_7 – J_{29} were found to be $|J_i| < 10$ K [34]. We calculated the J_i at $U = 7.19$ eV, where the mean-field Curie-Weiss temperature agrees with the experimental value $\Theta_{\text{CW}} = -165(1)$ K extracted from a fit of the inverse magnetic susceptibility [34]. The dominant exchange couplings, $J_4 = 120.1$ K, $J_5 = 211.6$ K and $J_6 = 367.7$ K form the non-uniform AFM kagome layers. Here, J_6 couples units of three Cu sites into trimers, similar to the motif deduced in Ref. [22] for in-plane exchange only [46, 47]. Smaller FM couplings $J_1 = -6.8$ K, $J_2 = -14.5$ K and $J_3 = -30.3$ K form the network to the interlayer sites, as suggested in Ref. [48].

Experimentally, the use of natural single-crystalline samples (details in Ref. [34]) allows us to resolve a complex sequence of magnetic phases/regions in zero and

weak magnetic fields ($\mathbf{H} \parallel b$ axis). As shown in Fig. 2(a), the magnetic specific heat c_{mag} [34] features an anomaly at 18.1 K in zero field, in full agreement with earlier results [20, 30]. Additionally, we observe two transition anomalies at 6.2 K and 6.4 K [inset Fig. 2(a)], not resolved as distinct maxima in previous polycrystal studies [30]. At 4.6 K, we detect a weak kink in the specific heat not reported before. The magnetic entropy S_{mag} at 18.1 K, obtained via an integration of c_{mag}/T [34], is only $\sim 1/3$ of $2R \ln(2)$, the entropy expected for two spin-1/2 per formula unit. The very sharp and intense 6.2 K-anomaly resembles that of a first-order phase transition.

Magnetometry in weak dc magnetic fields $\mathbf{H} \parallel b$ axis reveals different behavior below 6.2 K for field-cooled (FC) and zero-field cooled (ZFC) samples up to ~ 0.1 T [Fig. 2(b)] in accordance with earlier results for polycrystals [30]. At 4.7 K, slightly shifted from the temperature of the weak anomaly in the specific heat [Fig. 2(a)], the $M(T)$ -data feature a kink/maximum at 0.01 T (FC/ZFC). The magnetization anomaly at 18.1 K is very weak and is visible on a reduced scale only [inset Fig. 2(b)]. The ac magnetic susceptibility χ_{ac} [Fig. 2(c)] features an intense anomaly at 6.4 K for all frequencies studied ($\mu_0 H_{\text{dc}} = 0$ T, $\mu_0 H_{\text{ac}} = 0.5$ mT). A frequency-dependent behavior of $|\chi_{\text{ac}}|$ sets in at the 6.4 K anomaly and persists down to ~ 4.5 K, where a weak kink-like anomaly is present, not visible on the scale of Fig. 2(c). No anomaly can be resolved at 18.1 K. In Figs. 2(d)–(e), in-phase and out-of-phase components of the ac susceptibility, χ'_{ac} and χ''_{ac} , are plotted in the temperature region of the 6.2 K and 6.4 K transitions where the frequency dependence is most pronounced. Our observations are at variance with the behavior presented in the past for synthetic, polycrystalline clinoatacamite, where χ'_{ac} was found to be clearly frequency-dependent and χ''_{ac} to be non-zero even below 5 K [30]. Based on those earlier results, a spin-glass-like ground state was stated. Our results rule out spin-glassiness at low temperatures.

We complement the view on the zero-field sequence of phases/regions by carrying out single-crystal μ SR as well as neutron diffraction experiments. Zero-field (ZF) and weak transverse field (wTF) μ SR measurements were carried out using the General Purpose Surface-Muon Instrument [49] of the Swiss Muon Source at the Paul Scherrer Institut, Switzerland. μ SR clearly senses long-range magnetic order at temperature points below the 18.1 K transition. In wTF (30 G) at temperatures $T > 18.1$ K, in the paramagnetic phase, the whole asymmetry oscillates as the muon spins precess with the frequency of the external field [34]. Below 18.1 K the asymmetry in wTF is lost indicating that long-range order is present. Exemplary ZF asymmetry spectra as function of time taken at 1.73 K, 5.3 K and 10.8 K are presented in Fig. 3(a). They are typical for the temperature ranges below 4.6 K, above 6.4 K and the range between these two thermodynamic transitions, and they indicate different types of

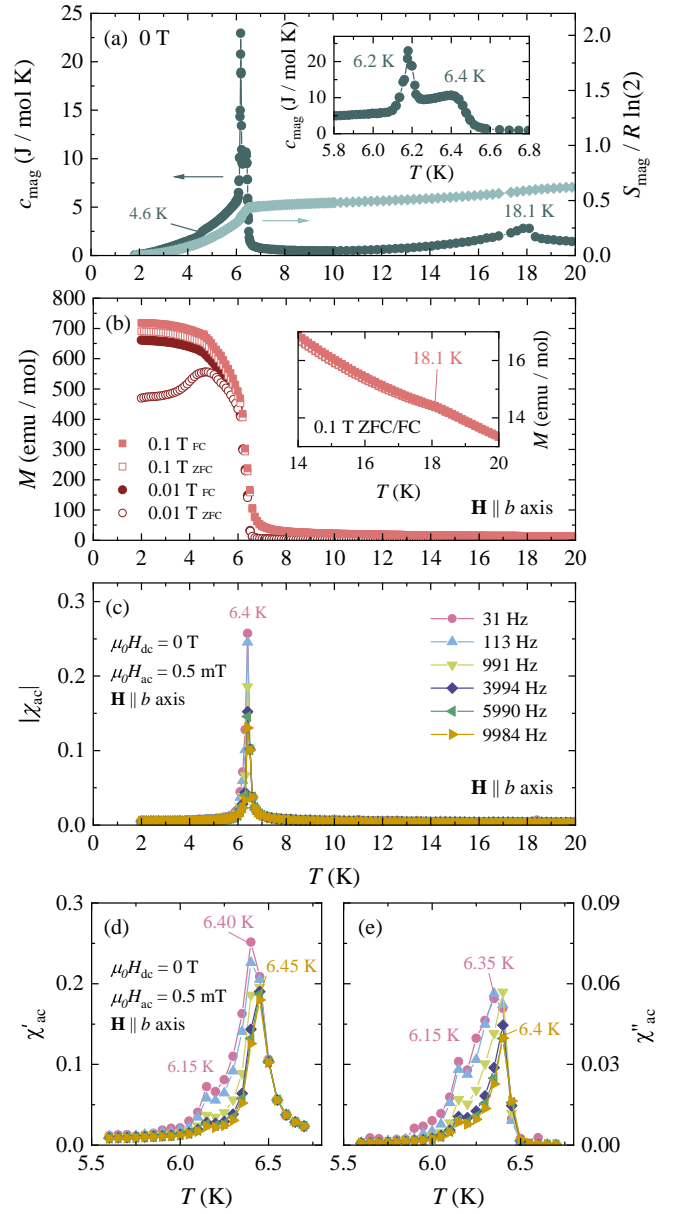


FIG. 2. (a) Magnetic specific heat c_{mag} and entropy S_{mag} in zero field and as function of temperature. The inset enlarges the region of the maxima at 6.2 K and 6.4 K. (b) Temperature dependence of the magnetization in weak dc magnetic fields (0.01 T, 0.1 T) for FC and ZFC samples ($\mathbf{H} \parallel b$ axis). The inset shows the subtle kink at 18.1 K in 0.1 T. (c) Temperature dependence of the magnitude of the ac magnetic susceptibility $|\chi_{\text{ac}}| = \sqrt{\chi_{\text{ac}}'^2 + \chi_{\text{ac}}''^2}$ with $\mu_0 H_{\text{dc}} = 0$ T and $\mu_0 H_{\text{ac}} = 0.5$ mT ($\mathbf{H} \parallel b$ axis) for various frequencies up to 9984 Hz. (d)–(e) In-phase and out-of-phase components of the ac susceptibility, χ'_{ac} and χ''_{ac} , in the region of the 6.2 K and 6.4 K anomalies.

long-range magnetic order. While above 6.4 K and below 4.6 K the experimental data can be well fitted to three distinct precession frequencies due to internal fields [34], the situation in the intermediate range is more complex with indications for enhanced spin dynamics sim-

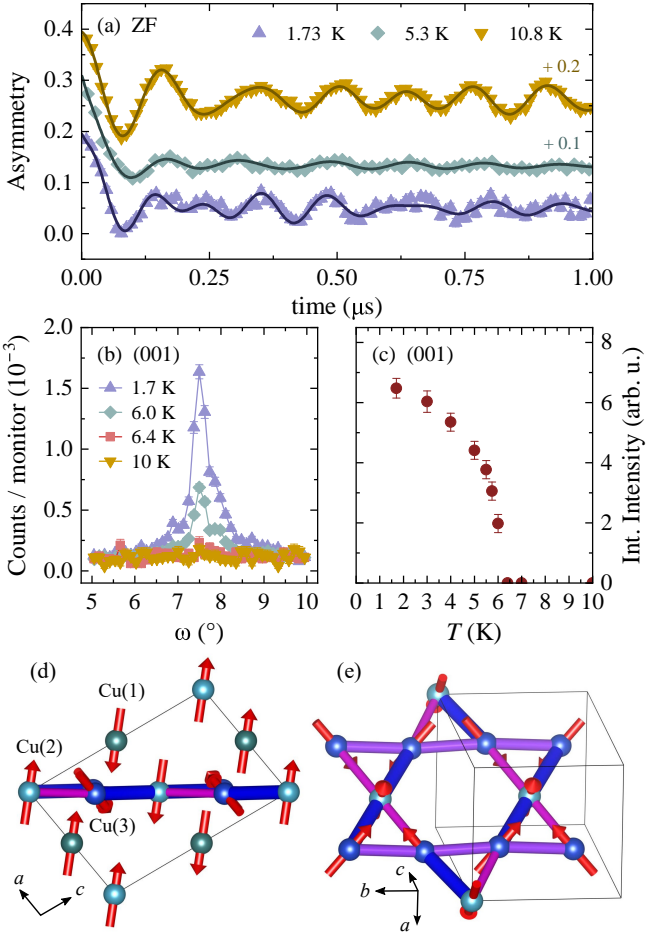


FIG. 3. (a) Zero-field μ SR asymmetry of single-crystalline clinoatacamite as function of time measured at 1.73 K, 5.3 K and 10.8 K. The data at 5.3 K and 10.8 K are shifted vertically. Solid lines are fits to the data; for details Ref. [34]. (b) Rocking curves of the purely magnetic (0 0 1) Bragg peak recorded at different temperatures on D10 ($\lambda = 2.36 \text{ \AA}$). Note: The peak has an asymmetric tail indicating a slight twinning of the crystal. (c) Integrated intensity of the magnetic (0 0 1) reflection as function of temperature. (d)–(e) Magnetic structure at 1.7 K [$R_M = 0.0545$ (in F)] together with the dominant couplings J_4 – J_6 . Views are (d) on the ac plane and (e) on a distorted kagome unit with Cu(2)/Cu(3) sites only.

ilar to the findings on polycrystalline material reported in Ref. [20]. An extensive analysis of our μ SR data with detailed discussion will be given elsewhere.

In agreement with previous results for deuterated clinoatacamite powder [21–23], our single-crystal neutron diffraction study reveals magnetic reflections below 6.4 K which are compatible with the magnetic propagation vector $\mathbf{q}_m = (0, 0, 0)$ [34]. The neutron diffraction experiments were carried out using the Four-Circle Diffractometer D10 of the Institut Laue-Langevin (ILL), France, as well as the Flat-Cone Diffractometer E2 [51] at BER II of HZB, Germany. As displayed in Figs. 3(b)–(c), the integrated intensity of the purely magnetic (0 0 1) re-

fraction decreases upon an increase of temperature and vanishes when stepping from 6.0 to 6.4 K, signaling the suppression of the $\mathbf{q}_m = (0, 0, 0)$ phase. Regarding the magnetic state present at higher temperatures, in Ref. [52], weak half-integer reflections were found at 7 K during a neutron diffraction study on deuterated powder, which were indexed with the magnetic propagation vector $\mathbf{q}_m = (-0.5, 0, 0.5)$. We can confirm the presence of corresponding reflections for single crystals from a recent test experiment on D10 [34, 53], and we plan to investigate the $\mathbf{q}_m = (-0.5, 0, 0.5)$ structure in the future.

Key to the determination of the magnetic structure in the low-temperature $\mathbf{q}_m = (0, 0, 0)$ phase was to measure the intensity of magnetic reflections, weak ones in particular, with good accuracy. This was limited in earlier powder studies [21–23], whereas single-crystal neutron diffraction allows to record the integrated intensities of individual Bragg peaks. Based on a corresponding experiment on D10 [54], we have carried out a refinement of the magnetic structure employing representation analysis [55–57] (details in Ref. [34]). We found that the data are best described [$R_M = 0.0545$ (in F)] using different irreducible representations for Cu(1)/Cu(2) on Wyckoff sites $2d/2a$ and Cu(3) on $4e$. The resulting magnetic structure is displayed in Figs. 3(d)–(e). The magnetic moments of Cu(1)/Cu(2) [58] lie in the ac plane with components of $\mu_{\text{ord,Cu}(1)}(x) = \mu_{\text{ord,Cu}(2)}(x) = 0.30(2) \mu_B$ and $\mu_{\text{ord,Cu}(1)}(z) = \mu_{\text{ord,Cu}(2)}(z) = 0.29(3) \mu_B$, resulting in a total moment of $\mu_{\text{ord,Cu}(1)} = \mu_{\text{ord,Cu}(2)} = 0.38(2) \mu_B$. The magnetic moments of Cu(3) lie in the ab plane with $\mu_{\text{ord,Cu}(3)}(x) = 0.29(2) \mu_B$ and $\mu_{\text{ord,Cu}(3)}(y) = 0.25(2) \mu_B$ resulting in a total moment of $\mu_{\text{ord,Cu}(3)} = 0.38(2) \mu_B$. The refinement yields collinear Cu(1)/Cu(2) moments, almost normal to the kagome plane, produced by an even-parity ordering mode (inversion-symmetric). The non-collinear Cu(3) moments are produced by an odd-parity ordering mode (broken inversion symmetry).

As the frustration of clinoatacamite is strong, below 18.1 K, these symmetry-different modes are expected to be close to multicriticality. This can be understood by considering the deformation of the underconstrained undistorted kagome antiferromagnet which supports many degenerate modes. Some of these modes must be connected with the distinct selected modes dominating magnetic ordering along the distortion path. From phenomenological Landau-theory for multicritical systems, one of the two competing modes should yield long-range order by a conventional continuous phase transition upon lowering temperature from the paramagnetic state. Eventually, a transition to a state of coexisting modes, or a domain state involving other modes could be seen in a bi- or tetracritical phase diagram [59].

From phenomenology of the multicritical system of modes, the behavior of clinoatacamite can be rationalized. Owing to the even and odd parity of the ordering modes, the magnetic free energy contains so-

called *Lifshitz-type* invariants (Lts), bilinear terms with one gradient [34]. These coupling terms allow the co-existence of symmetry-different modes in a common texture, a spatially modulated state in the order-parameter space as a homogeneous long-range order of one mode is destabilized against a spatially varying admixture of the other mode. The mechanism is similar to the rotation of the magnetization vector in a chiral helimagnet [60]. Such modulated mixtures of symmetry-different modes have been observed so far only in non-centrosymmetric magnetic crystals: as *metamagnetic texture*, a field-driven mixture of an AFM configuration with a FM state [31], while in a highly frustrated magnetic system similar textures have been invoked to explain the observation of quasi-static lumps of non-collinear spin-structures in absence of any long-range order [61]. The spin configuration below 6.4 K is a mixture of competing symmetry-different modes. This confirms the multicritical nature of magnetic ordering in clinoatacamite. Hence, the transition at 18.1 K could signal the formation of a textured state dominated by a primary mode frustrated by the closeness of another mode. The formation of such a partial order can explain the weak thermodynamic signature of this transition from the paramagnetic state. Consequently, the complex transition around 6.4 K appears to be triggered when the second ordering mode becomes thermodynamically stable upon lowering temperature. This process should reorganize the textured high-temperature state into a long-range ordered phase, which may explain the observation of a sequence of narrow intermediate or mesophase states at this transition.

In conclusion, clinoatacamite exemplifies a geometrically frustrated antiferromagnet where the existence of an underconstrained manifold of modes allows for a mechanism where competing modes can coexist and create textured magnetic states of mixed symmetry. The even/odd parity of the ordering modes is instrumental for such states. Such systems become exceedingly complex because of the multicriticality and the higher-level, i.e. non-local, frustration through the chiral Lifshitz invariants. In addition, in a low-symmetry crystal like clinoatacamite, many anisotropic coupling terms will influence its magnetic phase diagram.

Acknowledgements—We thank the Helmholtz-Zentrum Berlin für Materialien und Energie as well as the Institut Laue-Langevin for allocation of neutron radiation beamtime and thankfully acknowledge the financial support from HZB and ILL. This work is further based on experiments performed at the Swiss Muon Source SpS, Paul Scherrer Institute, Villigen, Switzerland. We thankfully acknowledge technical support from B. Veltel using the Physics Laboratory of MLZ. We thank T. Lampe for his support during the sample preparation, as well as J. L. Winter, K. Koschel and J. Willwater for their support in the early stages of this project. This work has partially been supported

by the DFG under Contract No. SU229/9-2, through SFB 1143 (Project No. 247310070) and Project No. 390858490 (Würzburg-Dresden Cluster of Excellence on Complexity and Topology in Quantum Matter-ct.qmat, EXC 2147). H. O. J. acknowledges support through JSPS KAKENHI Grants No. 24H01668 and No. 25K0846007. F. B. acknowledges support from the Agence Nationale de la Recherche (ANR), project ANR-25-CE30-2010-01. U. K. R. thanks U. Nitzsche for assistance with computational resources. Crystal and magnetic structures were drawn using VESTA 3 [62].

* Contact author: l.stoedter@fz-juelich.de

† Present address: Department of Physics, Federal University of Paraná, Curitiba, Paraná, Brazil

- [1] L. Balents, Spin liquids in frustrated magnets, *Nature* **464**, 199 (2010).
- [2] C. Broholm, R. J. Cava, S. A. Kivelson, D. G. Nocera, M. R. Norman, T. Senthil, Quantum Spin Liquids, *Science* **367**, eaay0668 (2020).
- [3] P. Mendels, F. Bert, M. A. de Vries, A. Olariu, A. Harrison, F. Duc, J. C. Trombe, J. S. Lord, A. Amato, and C. Baines, Quantum Magnetism in the Paratacamite Family: Towards an Ideal Kagomé Lattice, *Phys. Rev. Lett.* **98**, 077204 (2007).
- [4] M. R. Norman, *Colloquium*: Herbertsmithite and the search for the quantum spin liquid, *Rev. Mod. Phys.* **88**, 041002 (2016).
- [5] P. Khuntia, M. Velázquez, Q. Barthélémy, F. Bert, E. Kermarrec, A. Legros, B. Bernu, L. Messio, A. Zorko, and P. Mendels, Gapless ground state in the archetypal quantum kagomé antiferromagnet $ZnCu_3(OH)_6Cl_2$, *Nat. Phys.* **16**, 469 (2020).
- [6] E. Kermarrec, P. Mendels, F. Bert, R. H. Colman, A. S. Wills, P. Strobel, P. Bonville, A. Hillier, and A. Amato, Spin-liquid ground state in the frustrated kagomé antiferromagnet $MgCu_3(OH)_6Cl_2$, *Phys. Rev. B* **84**, 100401(R) (2011).
- [7] D. Boldrin, B. Fåk, M. Enderle, S. Bieri, J. Ollivier, S. Rols, P. Manuel, and A. S. Wills, Haydeeite: A spin-1/2 kagomé ferromagnet, *Phys. Rev. B* **91**, 220408(R) (2015).
- [8] P. Puphal, K. M. Zoch, J. Désor, M. Bolte, and C. Krellner, Kagomé quantum spin systems in the atacamite family, *Phys. Rev. Mater.* **2**, 063402 (2018).
- [9] R. Okuma, D. Nakamura, T. Okubo, A. Miyake, A. Matsuo, K. Kindo, M. Tokunaga, N. Kawashima, S. Takeyama, and Z. Hiroi, A series of magnon crystals appearing under ultrahigh magnetic fields in a kagomé antiferromagnet, *Nat. Commun.* **10**, 1229 (2019).
- [10] A. Henderson, L. Dong, S. Biswas, H. I. Revell, Y. Xin, R. Valenti, J. A. Schlueter, and T. Siegrist, Order-disorder transition in the $S = 1/2$ kagomé antiferromagnets clarinbullite and barlowite, *Chem. Commun.* **55**, 11587 (2019).
- [11] M. Akazawa, M. Shimozawa, S. Kittaka, T. Sakakibara, R. Okuma, Z. Hiroi, H.-Y. Lee, N. Kawashima, J. H. Han, and M. Yamashita, Thermal Hall Effects of Spins and Phonons in Kagomé Antiferromagnet Cd-Kapellasite *Phys. Rev. X* **10**, 041059 (2020).

[12] K. Tustain, E. E. McCabe, A. M. Arevalo-Lopez, A. S. Gibbs, S. P. Thompson, C. A. Murray, C. Ritter and L. Clark, Disorder-Induced Structural Complexity in the Barlowite Family of $S = 1/2$ Kagomé Magnets, *Chem. Mater.* **33**, 24, 9638 (2021).

[13] D. Chatterjee, P. Puphal, Q. Barthélémy, J. Willwater, S. Süllow, C. Baines, S. Petit, E. Ressouche, J. Ollivier, K. M. Zoch, C. Krellner, M. Parzer, A. Riss, F. Garmroudi, A. Pustogow, P. Mendels, E. Kermarrec, and F. Bert, From spin liquid to magnetic ordering in the anisotropic kagomé Y-kapellasite $Y_3Cu_9(OH)_{19}Cl_8$: A single-crystal study, *Phys. Rev. B* **107**, 125156 (2023).

[14] J. Wang, M. Spitaler, Y.-S. Su, K. M. Zoch, C. Krellner, P. Puphal, S. E. Brown, and A. Pustogow, Controlled Frustration Release on the Kagomé Lattice by Uniaxial-Strain Tuning, *Phys. Rev. Lett.* **131**, 256501 (2023).

[15] K. Matan, T. Ono, Y. Fukumoto, T. J. Sato, J. Yamaura, M. Yano, K. Morita, and H. Tanaka, Pinwheel valence-bond solid and triplet excitations in the two-dimensional deformed kagomé lattice, *Nat. Phys.* **6**, 865 (2010).

[16] M. S. Grbić, S. Krämer, C. Berthier, F. Trouselet, O. Cépas, H. Tanaka, and M. Horvatić, Microscopic Properties of the Pinwheel Kagomé Compound $Rb_2Cu_3SnF_{12}$, *Phys. Rev. Lett.* **110**, 247203 (2013).

[17] M. Hering, F. Ferrari, A. Razpopov, I. I. Mazin, R. Valentí, H. O. Jeschke, and J. Reuther, Phase diagram of a distorted kagomé antiferromagnet and application to Y-kapellasite, *npj Comput Mater* **8**, 10 (2022).

[18] O. Janson, S. Furukawa, T. Momoi, P. Sindzingre, J. Richter, and K. Held, Magnetic Behavior of Volborthite Determined by Coupled Trimers Rather than Frustrated Chains, *Phys. Rev. Lett.* **117**, 037206 (2016).

[19] K. Matan, T. Ono, G. Gitgeatpong, K. de Roos, P. Miao, S. Torii, T. Kamiyama, A. Miyata, A. Matsuo, K. Kindo, S. Takeyama, Y. Nambu, P. Piyawongwatthana, T. J. Sato, and H. Tanaka, Magnetic structure and high-field magnetization of the distorted kagomé lattice antiferromagnet $Cs_2Cu_3SnF_{12}$, *Phys. Rev. B* **99**, 224404 (2019).

[20] X. G. Zheng, H. Kubozono, K. Nishiyama, W. Higemoto, T. Kawae, A. Koda, and C. N. Xu, Coexistence of Long-Range Order and Spin Fluctuation in Geometrically Frustrated Clinoatacamite $Cu_2Cl(OH)_3$, *Phys. Rev. Lett.* **95**, 057201 (2005).

[21] S.-H. Lee, H. Kikuchi, Y. Qiu, B. Lake, Q. Huang, K. Habicht, and K. Kiefer, Quantum-spin-liquid states in the two-dimensional kagomé antiferromagnets $Zn_xCu_{4-x}(OD)_6Cl_2$, *Nat. Mater.* **6**, 853 (2007).

[22] J.-H. Kim, S. Ji, S.-H. Lee, B. Lake, T. Yildirim, H. Nojiri, H. Kikuchi, K. Habicht, Y. Qiu, and K. Kiefer, External Magnetic Field Effects on a Distorted Kagomé Antiferromagnet, *Phys. Rev. Lett.* **101**, 107201 (2008).

[23] A. S. Wills and J.-Y. Henry, On the crystal and magnetic ordering structures of clinoatacamite, γ - $Cu_2Cl(OH)_3$, a proposed valence bond solid, *J. Phys.: Condens. Matter* **20**, 472206 (2008).

[24] A. S. Wills, T. G. Perring, S. Raymond, B. Fåk, J.-Y. Henry, and M. Telling, Inelastic neutron scattering studies of the quantum frustrated magnet clinoatacamite, γ - $Cu_2(OD)_3Cl$, a proposed valence bond solid (VBS), *J. Phys.: Conf. Ser.* **145**, 012056 (2009).

[25] S. Maegawa, A. Oyamada, and S. Sato, Novel Frustrated Behavior in Quantum Heisenberg Antiferromagnets on the Pyrochlore Lattice: NMR Studies of $R_2(OH)_3Cl$ ($R = Cu$ and Ni), *J. Phys. Soc. Jpn.* **79**, 011002 (2010).

[26] H. Morodomi, K. Ienaga, Y. Inagaki, T. Kawae, M. Hagiwara, X. G. Zheng, Specific heat study of geometrically frustrated magnet clinoatacamite $Cu_2Cl(OH)_3$, *J. Phys.: Conf. Ser.* **200**, 032047 (2010).

[27] H. Morodomi, K. Ienaga, Y. Inagaki, T. Kawae, M. Hagiwara, X. G. Zheng, Magnetic Field dependence of specific heat in Clinoatacamite $Cu_2Cl(OH)_3$, *J. Phys.: Conf. Ser.* **400**, 032058 (2012).

[28] In the past, magnetic studies on clinoatacamite were carried out using synthesized (in part deuterated) as well as natural polycrystals and powder [20–27, 29, 30], however, the results yielded an inconsistent picture. It was found that clinoatacamite undergoes a magnetic transition at 18.1 K, signaled by weak anomalies of the magnetic susceptibility and the heat capacity as well as by the onset of oscillations of the μ SR asymmetry [20, 30]. An additional transition was reported to occur at 6.2 K [20]. Zero-field μ SR measurements in this lower-temperature region revealed oscillations of the asymmetry only at lowest temperatures ~ 2 K [20]. Powder neutron scattering of deuterated material supported long-range magnetic order with a propagation vector $\mathbf{q}_m = (0, 0, 0)$ below 6.7 K [21, 22]. Curiously, no magnetic reflections were found at higher temperatures and up to 18.1 K, where μ SR sensed long-range magnetic order [20]. From the flat band of excitations observed for deuterated clinoatacamite powder by means of inelastic neutron scattering at 1.5 K, in Ref. [21] it was concluded on a valence-bond solid ground state.

[29] A. S. Wills, S. Raymond, and J.-Y. Henry, Magnetic ordering in a distorted $S = \frac{1}{2}$ pyrochlore antiferromagnet, *J. Magn. Magn. Mater.* **272–276**, 850 (2004).

[30] X. G. Zheng, T. Kawae, Y. Kashitani, C. S. Li, N. Tateiwa, K. Takeda, H. Yamada, C. N. Xu, and Y. Ren, Unconventional magnetic transitions in the mineral clinoatacamite $Cu_2Cl(OH)_3$, *Phys. Rev. B* **71**, 052409 (2005).

[31] D. A. Sokolov, N. Kikugawa, T. Helm, H. Borrmann, U. Burkhardt, R. Cubitt, J. S. White, E. Ressouche, M. Bleuel, K. Kummer, A. P. Mackenzie, and U. K. Rößler, Metamagnetic texture in a polar antiferromagnet, *Nat. Phys.* **15**, 671 (2019).

[32] J. D. Grice, J. T. Szymański, and J. L. Jambor, The crystal structure of clinoatacamite, a new polymorph of $Cu_2Cl(OH)_3$, *Can. Mineral.* **34**, 73 (1996).

[33] T. Malcherek and J. Schlüter, Structures of the pseudo-trigonal polymorphs of $Cu_2(OH)_3Cl$, *Acta Cryst. B* **65**, 334 (2009).

[34] See Supplemental Material at (URL will be inserted by publisher) for additional information on the structural characterization of clinoatacamite, the derivation of the motif of exchange couplings, the thermodynamic measurements, the μ SR data analysis, the neutron diffraction experiments and the magnetic structure determination as well as the discussion of the phenomenological magnetic free energy. The Supplemental Material contains Refs. [35–38].

[35] L. Heinze, R. Beltran-Rodriguez, G. Bastien, A. U. B. Wolter, M. Reehuis, J.-U. Hoffmann, K. C. Rule, and S. Süllow, The magnetic properties of single-crystalline atacamite, $Cu_2Cl(OH)_3$, *Physica B* **536**, 377 (2018).

[36] D. Guterding, R. Valentí, and H. O. Jeschke, Reduction of magnetic interlayer coupling in barlowite through iso-electronic substitution, *Phys. Rev. B* **94**, 125136 (2016).

[37] Y. Iqbal, H. O. Jeschke, J. Reuther, R. Valentí, I. I. Mazin, M. Greiter, and R. Thomale, Paramagnetism in the kagome compounds $(\text{Zn,Mg,Cd})\text{Cu}_3(\text{OH})_6\text{Cl}_{12}$, *Phys. Rev. B* **92**, 220404(R) (2015).

[38] G. N. Iles, and S. Schorr, The HZB neutron Laue diffractometer: From E11 to FALCON, *Neutron News* **25**, 27 (2014).

[39] K. Koepernik and H. Eschrig, Full-potential nonorthogonal local-orbital minimum-basis band-structure scheme, *Phys. Rev. B* **59**, 1743 (1999).

[40] J. P. Perdew, K. Burke, and M. Ernzerhof, Generalized Gradient Approximation Made Simple, *Phys. Rev. Lett.* **77**, 3865 (1996).

[41] A. I. Liechtenstein, V. I. Anisimov, and J. Zaanen, Density-functional theory and strong interactions: Orbital ordering in Mott-Hubbard insulators, *Phys. Rev. B* **52**, R5467(R) (1995).

[42] S. R. Hall, G. S. D. King, J. M. Stewart, Eds., *Xtal 3.4 User's Manual*. University of Australia: Lamb, Perth (1995).

[43] V. F. Sears, in *International Tables for Crystallography*, edited by A. J. C. Wilson (Kluwer Academic Publishers, Dordrecht/Boston/London, 1995), Vol. C, p. 383.

[44] V. F. Sears, Neutron scattering lengths and cross sections, *Neutron News* **3**, 26 (1992).

[45] W. H. Zachariasen, A general theory of X-ray diffraction in crystals, *Acta Cryst.* **23**, 558 (1967).

[46] Note that this motif of exchange couplings in the kagome plane was formerly studied in Ref. [47], a study motivated by the coupling motif of clinoatacamite, but where the case $J_6 \gg J_4, J_5$ (our notation) was treated.

[47] A. B. Harris and T. Yildirim, Spin dynamics of trimers on a distorted kagome lattice, *Phys. Rev. B* **88**, 014411 (2013).

[48] E. Khatami, J. S. Helton, and M. Rigol, Numerical study of the thermodynamics of clinoatacamite, *Phys. Rev. B* **85**, 064401 (2012).

[49] A. Amato, H. Luetkens, K. Sedlak, A. Stoykov, R. Scheuermann, M. Elender, A. Raselli, D. Graf, The new versatile general purpose surface-muon instrument (GPS) based on silicon photomultipliers for μ SR measurements on a continuous-wave beam, *Rev. Sci. Instrum.* **88**, 093301 (2017).

[50] A. Suter, and B. M. Wojek, Musrfit: A Free Platform-Independent Framework for μ SR Data Analysis, *Phys. Proc.* **30**, 69 (2012).

[51] Helmholtz-Zentrum Berlin für Materialien und Energie, E2: The Flat-Cone Diffractometer at BER II, *J. Large-Scale Res. Facil.* **4**, A129 (2018).

[52] X.-G. Zheng, M. Hagihala, I. Yamauchi, E. Nishibori, T. Honda, T. Yuasa, and C.-N. Xu, A novel Kagome unddu spin order in Heisenberg spin-1/2 Clinoatacamite $\text{Cu}_4(\text{OH})_6\text{Cl}_2$, the parent compound of Herbertsmithite, [arXiv:2411.01277](https://arxiv.org/abs/2411.01277) [cond-mat.str-el].

[53] E. Chan, Institut Laue-Langevin (ILL), <https://doi.org/10.5291/ILL-DATA.EASY-1612> (2025).

[54] L. Stödter, K. Beauvois, B. Ouladdiaf, M. Reehuis, T. Reimann, K. C. Rule, S. Süllow, and A. U. B. Wolter, Institut Laue-Langevin (ILL), <https://doi.org/10.5291/ILL-DATA.5-41-1083> (2021).

[55] E. F. Bertaut, Representation analysis of magnetic structures, *Acta Cryst. A* **24**, 217 (1968).

[56] J. Rodríguez-Carvajal, Recent advances in magnetic structure determination by neutron powder diffraction, *Physica B* **192**, 55 (1993).

[57] P. J. Brown, in *International Tables for Crystallography*, edited by A. J. C. Wilson (Kluwer Academic Publishers, Dordrecht/Boston/London, 1995), Vol. C, p. 391.

[58] During the refinement we treated $\text{Cu}(1)/\text{Cu}(2)$ as one magnetic sublattice as they share site symmetry $\bar{1}$.

[59] P. M. Chaikin and T. C. Lubensky, *Principles of Condensed Matter Physics*, Cambridge UP, Cambridge UK (1995).

[60] I. E. Dzyaloshinskii, Sov. Phys. JETP **19**, 960 (1964).

[61] W. Schweika, M. Valldor, J. D. Reim, and U. K. Rößler, Chiral spin liquid ground state in $\text{YBaCo}_3\text{FeO}_7$, *Phys. Rev. X* **12**, 021029 (2022).

[62] K. Momma and F. Izumi, VESTA 3 for three-dimensional visualization of crystal, volumetric and morphology data, *J. Appl. Cryst.* **44**, 1272 (2011).